J Appl Electrochem (2011) 41:1005–1012
DOI 10.1007/s10800-011-0334-8

ORIGINAL PAPER

Micro-tubular solid oxide fuel cells fabricated from hollow fibres

N. Droushiotis · U. Doraswami · G. H. Kelsall · K. Li

Received: 22 January 2011 / Accepted: 9 July 2011 / Published online: 5 August 2011

Abstract Recent literature is reviewed on a phase inversion process followed by sintering, used to fabricate ceramic hollow fibres (HFs) as precursors to micro-tubular solid oxide fuel cells (MT-SOFCs) with sub-millimetre inner diameters. These aimed to address the outstanding technological and economic issues that have delayed mass production of SOFCs, by increasing electrode surface areas per unit volume relative to planar structures, increasing power outputs per unit volume/mass, facilitating sealing at high temperatures, and decreasing fabrication costs per kW. Some recent experimental results are presented of the effects of temperature, hydrogen flow rate, thermal cycling and time of NiO reduction with H_2 on the subsequent performance of 25 mm long H_2|Ni–CGO|CGO|LSCF|air MT-SOFCs, incorporating cerium–gadolinium oxide (CGO) electrolyte, nickel anodes and lanthanum strontium cobalt ferrite–CGO (LSCF–CGO) cermet cathodes, designed to operate at 500–600 °C. Maximum power densities of 3–5.5 kW m^{-2} were achieved as the temperature was increased from 550–600 °C. The co-extruded MT-SOFCs were resilient to three thermal cycles when heated to operating temperature in ca. 5 min. Their performance was intimately related to the reduction time, suggesting slow conversion of the NiO to Ni within the fabricated anodes. At constant cell voltage, mass transport limited current densities increased from ca. 11 to ca. 13.5 kA m^{-2} as hydrogen flow rates were increased from 15 to 60 cm^3 min^{-1}, though had residual NiO in the anode been fully reduced, current densities would have been significantly greater.

Keywords Solid oxide fuel cells (SOFCs) · Hollow fibres · Micro-tubular SOFCs · Cerium–gadolinium oxide (CGO) · Lanthanum strontium cobalt ferrite (LSCF)

1 Introduction

Solid oxide fuel cells (SOFCs) have an enormous market potential, because they can convert chemical to electrical energy directly with energy efficiencies greater than achievable by fossil-fuelled electrical power stations, and are environmentally benign in operation, since (hydrogen–oxygen) fuel cells emit only water. However, their mass production has been delayed because of outstanding technological and economic issues. The project, for which results are presented below, aimed to solve some of these problems by developing a novel design of so-called micro-tubular SOFCs (MT-SOFCs). These were fabricated using hollow fibres (HFs) with sub-millimetre inner diameters, thereby increasing electrode surface areas per unit volume relative to planar structures, increasing power outputs per unit volume/mass, facilitating sealing at high temperatures, and decreasing fabrication costs per kW. Phase inversion, followed by sintering of metal oxide precursors, was used to produce HFs with controlled microstructures, eminently suitable for fabricating electrolyte [1] and anode-supported tubular SOFCs [2]. Such small tubes also appear to have mechanical properties superior to counterparts with larger diameters. Micro-tubular SOFCs, the subject of a recent review [3], may be easier to seal at operating temperatures than their planar counterparts and are less susceptible to

N. Droushiotis · U. Doraswami · G. H. Kelsall (✉) · K. Li
Department of Chemical Engineering, Imperial College London, London SW7 2AZ, UK
e-mail: g.kelsall@imperial.ac.uk

thermal stresses resulting from rapid changes in power, making them potentially suitable for transport applications. However, axial potential losses and current collector and inter-connect designs are greater problems for tubular SOFCs [4].

The two principal SOFC designs, planar and tubular, have been researched extensively and are being developed commercially, e.g. by NexTech, AMI Inc., Acumentrics etc. and by Bloom Energy and Ceres Power Ltd. in the former case; decreasing cell fabrication costs per kW would aid the commercialisation of both designs. Yttria-stabilised zirconia (YSZ) and ceria–gadolinia [5] are the most commonly used electrolytes, which require operating temperatures of 750–1000 and 500–600 °C, respectively, to minimise ohmic potential losses and hence maximise power densities.

Firstly, HF YSZ electrolytes were fabricated by a spinning/phase inversion process [6, 7], followed by sintering, to produce thin (10–100 μm), dense, gas-tight layers, with integrated porous super-layers ca. 50–100 μm thick on both sides [1]. From e.g. YSZ suspensions, electrolyte-supported structures were produced; after sintering of the fibres, nickel was deposited electrolessly onto their inner surfaces to form Ni–YSZ anodes. Lanthanum strontium manganite (LSM)–YSZ cathodes were then coated onto outer surfaces of the fibres. Anode ('electroless' nickel) and cathode (LSM) materials were deposited onto these porous super-layers on either side of the electrolyte-supported structure to produce single MT-SOFCs. Their performances, reducing atmospheric oxygen at the cathode and oxidising hydrogen to water vapour at the anode, were determined as a function of the fabrication and operational parameters.

The effects of geometric design and experimental variables on MT-SOFC performance was explored using 3D finite element models [4, 8, 9] of single H_2|Ni–YSZ|YSZ|LSM|air MT-SOFCs and multiple MT-SOFCs connected in series for voltage scale-up and parallel for current scale-up; sufficient kinetic and physical property data were available in the literature only for YSZ-based systems. The equations were solved using COMSOL Multiphysics™ (www.comsol.com) to aid reactor design, focus experimental work and to understand better how to optimise the performance of individual MT-SOFCs and bundles. Results from the mathematical models were used to optimise current collection geometry and to better understand the effect of current distributions on cell performance for a range of geometries and operating conditions. For pairs of current collectors at both ends of cells, the models predicted decreasing average currents as MT-SOFC lengths were increased, due to increasing potential drops axially along electrodes, affecting maximum power densities greatly.

Hence, to obviate problems of 'electroless' nickel deposition on inner surfaces of electrolyte micro-tubes leading to low axial electronic conductivities and decreasing porosities, anode-supported MT-SOFCs were produced [2].

After modification of the spinneret system for producing HFs, the feasibility was then demonstrated of co-extruding anode/electrolyte structures in a single phase inversion process [10–13], as shown schematically in Fig. 1. This minimizes sintering steps and fabrication times, compared with single layer extrusion methods, while still enabling control of the thickness of the gas-tight electrolyte layer and the morphology of the overlying porous electrodes. After co-sintering, only deposition of particulate precursors of the cathode, followed by further sintering, was required to fabricate a complete MT-SOFC, thereby simplifying the overall fabrication process and further decreasing costs. Compared with conventional ram extrusion, such processes should decrease unit costs, especially at mass production scales, enable better control of internal structures of extruded layers, and impose minimal restrictions on fibre lengths and diameters. Furthermore, the use of phase inversion and sintering produces supporting substrates with various microstructures that affect power densities of MT-SOFCs directly [14].

Most experiments have focused on co-extrusion by phase inversion of NiO–$Ce_{0.9}Gd_{0.1}O_{1.95}$ (CGO) as anode precursors and cerium–gadolinium oxide (CGO) as electrolyte simultaneously [2, 10–13, 16]. The NiO was reduced at 550 °C using hydrogen to form Ni anodes, which had greater axial electronic conductivities and better distribution of active Ni than the Ni deposited electrolessly in their electrolyte-supported counterparts, increasing 'triple phase boundary lengths' within the anode. Graded CGO–$La_{0.6}Sr_{0.4}Co_{0.2}Fe_{0.8}O_3$ (LSCF) particles were deposited by spray painting, dip-coating or electrophoretic

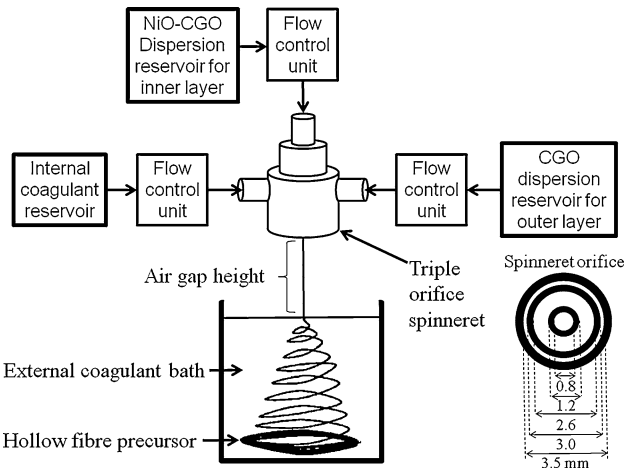

Fig. 1 Schematic of phase inversion process used to produce NiO–CGO anode/CGO electrolyte HFs using triple orifice spinneret [6]

deposition, then sintered to form the cathodes of short (10–50 mm) individual MT-SOFCs, the performances of which were determined as functions of fabrication conditions and operational parameters. The CGO electrolyte [16] enabled operating temperatures to be decreased to 500–600 °C from ca. 900 °C for YSZ electrolytes. The use of 'graded' cathodes, higher porosity anodes [17] and improved anode current collection methods enhanced the performance of such fuel cells, which produced maximum power densities of 1186, 2193, 4470 and 5864 at 450, 500, 550 and 570 °C, respectively.

Using focussed ion beam—scanning electron microscopy image reconstruction of the anode, triple phase boundary densities were estimated and used in the model to better understand the spatial distributions of current densities [18].

The fabrication of micro-tubular SOFCs using HFs has been adopted by others, producing NiO–YSZ anode precursors [19–22], in the last case coupled to a 'redox stable' $(La_{0.75}Sr_{0.25})_{0.95}Cr_{0.5}Mn_{0.5}O_{3-\delta}$–$Sm_{0.2}Ce_{0.8}O_{1.9}$–YSZ composite cathode, enabling a peak power density of 2.78–5.13 kW m^{-2} to be achieved at 750–850 °C. In addition, asymmetrically structured porous NiO–YSZ HF substrates have been dip-coating with dense YSZ electrolyte, on which porous strontium doped LSM-YSZ oxygen electrode was deposited and impregnated with samarium doped ceria (SDC—$Sm_{0.2}Ce_{0.8}O_{1.9}$) catalyst [23]. The resulting LSM–SDC–YSZ/YSZ/Ni–YSZ micro-tubular solid oxide cell achieved maximum power densities of 5.4, 7.1 and 12.5 kW m^{-2} at 800, 850 and 900 °C, respectively in fuel cell mode. In electrolysis mode at 900 °C with an applied potential difference of 1.3 V, current densities of 6.8 and 25.7 kA m^{-2} were obtained at 30 and 80 vol.% humidity, respectively.

Immersion-induced phase inversion has also been used to produce ca. 20 μm thick NiO–$BaZr_{0.1}Ce_{0.7}Y_{0.1}Yb_{0.1}O_{3-x}$ HFs [24] with asymmetric structures consisting of finger-like and sponge-like porous layers, onto which $BaZr_{0.1}Ce_{0.7}Y_{0.1}Yb_{0.1}O_{3-x}$ proton-conducting electrolytes were deposited after reduction of the NiO to produce Ni–$BaZr_{0.1}Ce_{0.7}Y_{0.1}Yb_{0.1}O_{3-x}$ anodes. A porous $Sm_{0.5}Sr_{0.5}CoO_3$-$BaZr_{0.1}Ce_{0.7}Y_{0.1}Yb_{0.1}O_{3-x}$ cathode was applied to the electrolyte by slurry coating. The resulting micro-tubular proton-conducting SOFC generated a peak power density of 2.54 kW m^{-2} at 650 °C. None of these studies used co-extrusion to produce anode and electrolyte precursors simultaneously, unlike those reported in [2, 10–13, 16].

Conventional ram extrusion of anode and/or electrolyte has been pioneered by Kendall [25] and by Suzuki et al. [26, 27], who has achieved power densities of 10 kW m^{-2} using CGO electrolytes. However, extrusion of micro-tubes becomes more problematic with decreasing diameter, required to achieve higher volumetric power densities, and with increasing length.

2 Experimental

NiO–CGO/CGO anode/electrolyte HFs of controlled anode microstructure and inner diameters of ca. 1 mm were prepared by phase inversion and sintering [11]. After co-sintering the NiO–CGO/CGO anode/electrolyte at 1550 °C, the dual-layer anode fibre retained a microstructure consisting of large finger-like pores at the inner surface and smaller sponge-like pores toward the electrolyte throughout the remaining anode thickness. Multiple layers of lanthanum strontium cobalt ferrite (LSCF)–CGO particles dispersed in ethylene glycol were deposited on the electrolyte layer by slurry coating using a paint brush to form a graded cathode layer, which was sintered at 1,200 °C for 4 h. Compositionally 'graded' cathodes, containing increasing concentration of LSCF, as the current collector was approached radially from the electrolyte/cathode interface, were deposited by spray painting, dip coating or electrophoretic deposition of different slurries of LSCF–CGO. The last slurry forming the outermost surface of the cathode was pure LSCF, to increase electronic conductivity at the electrode/current collector interface.

Silver wire (Alfa Aesar, UK) was wrapped around the 25 mm long cathode and conductive platinum paste (SPI Supplies Platinum Paint, USA) was used to improve the connection to the cathode surface and minimise potential drops at the cathode | current collector interface during the MT-SOFC test. Silver wool was packed inside the fibre lumen to collect the anode current, producing excellent electrical contact onto the anode wall, minimising anode | current collector ohmic potential losses. The high porosity of the wool ensured reactant and product mass transfer at the anode was not unduly restricted. The fabricated MT-SOFC was attached to an alumina tube using high temperature cement (Aremco, USA) before being sealed in a quartz tube that served as the air flow chamber. Details of the reactor and test apparatus used are provided elsewhere [11]. The MT-SOFC anode was supplied with controlled flows of hydrogen from a cylinder that was humidified by passing it through a water bath before being fed to the fuel cell while the cathode was supplied with a fixed air flow rate using mass flow controllers (Bronkhorst, UK).

The electrochemical performances of MT-SOFCs at operating temperatures between 500 and 600 °C in a tube furnace (Carbolite VST-HST 1200) were determined using a Metrohm PGSTAT302 potentiostat/galvanostat with a 10 A current booster.

The performance of the MT-SOFC was recorded at different intervals after starting the hydrogen flow, corresponding to varied anode reduction times, in order to quantify minimum times required to completely activate the NiO–YSZ anode. To investigate the reduction of NiO with hydrogen further, single layer 60 wt% NiO–40 wt% CGO fibres were sintered using the same sintering profile as for the dual-layer fibres. Then ceramic tubes (Multilab Ceramics, UK) were sealed to each end of the fibres with cement (Aremco, USA) to feed hydrogen and exhaust product water vapour and unreacted hydrogen. The structure, supported on another ceramic tube, was enclosed in a quartz tube, fed with high purity nitrogen, so that hydrogen escaped from the porous anode and the outer surface was exposed to an 'oxygen-free' N_2 atmosphere to prevent oxidation of the nickel. Hydrogen was flowed at 5 cm^3 min^{-1} and 550 °C (or 500 °C) for 30, 70 and 150 min through the ceramic tubes and inside the anode fibre only, as during MT-SOFCs experiments. The partially reduced fibres were cooled in H_2 or N_2 from 550 °C to room temperature, to minimise re-oxidation of the Ni.

Subsequently, samples were analysed by X-ray diffraction XRD and SEM to determine semi-quantitatively the residual NiO, using the unreacted Gd_2O_3 as a reference. XRD measurements were made using an X'celerator detector, Soller slit 0.04 rad (X'Pert PRO model, PANalytical, UK) and a Cu X-ray tube with Kα radiation ($\lambda = 154.2$ pm). The sintered samples were analyzed in the range of $5° \leq 2\theta \leq 80°$ with a step size of 0.0167° and a scan speed of 0.0301 s^{-1}. The tube voltage was 40 kV and the current set to 40 mA.

A Leo Gemini 1525 field emission gun scanning electron microscope (FEGSEM), at 5 kV and a working distance of 5–6 mm for in-lens secondary electron (SE) imaging, was used to image the microstructures of electrodes and electrode/ electrolyte interfaces from MT-SOFCs.

3 Results and discussion

3.1 MT-SOFC microstructures

Figure 2a–c show photomicrographs of the cross section of a MT-SOFC, with ca. 230 μm porous Ni–CGO inner anode layer, ca. 80 μm dense CGO electrolyte and ca. 30 μm outer porous LSCF cathode.

The cathode layer was well-bonded to the CGO electrolyte with no apparent delamination at either anode or cathode. The anode microstructure consisted of two clear zones: finger-like pores close to the fibre lumen penetrating toward the electrolyte for ca. 30% of the anode thickness, and a denser 'active' layer consisting of distributed sponge-like pores, to maximise Ni–CGO–fuel triple phase boundary lengths.

3.2 Effect of temperature on MT-SOFC performance

Figure 3 shows the effect of current density and temperature on the cell voltage and power densities for a 25 mm long H_2|Ni–CGO|CGO|LSCF|air MT-SOFC at a H_2 flow rate of 15 cm^3 min^{-1}; the NiO anode precursor had been reduced for 150 min at 550 °C. Experiments were conducted in order of increasing temperature with scan rates of ca. 10 mA s^{-1}, so that the time for the experiment itself caused minimal further reduction of the NiO in the anode. As expected, increasing temperature (T) in the range 550–600 °C increased cell voltages (U) and power densities (PD), at least for (anode) current densities (j) > 1 kA m^{-2}, due to decreased overpotentials in the electrodes and ohmic potential losses $\left(\Delta\phi_{CGO,T} = \bar{j} \cdot d_{CGO}/\kappa_{CGO,T}\right)$ in the CGO electrolyte, the latter caused by increased ionic conductivities $\left(\kappa_{CGO,T}\right)$ of CGO. In the above equation $\bar{j}$ represents the average current density and d_{CGO} the thickness of the electrolyte layer. However, the increased electronic conductivity of CGO, a mixed ionic-electronic conductor, partially shorting the MT-SOFC, precluded using higher temperatures.

At current densities <1 kA m^{-2}, Fig. 3 shows that cell voltages were higher at lower temperatures, probably due to a combination of the equilibrium potential differences increasing with decreasing temperature (Fig. 4) and the increased magnitudes of the leakage currents across the CGO electrolyte at higher temperatures decreasing the MT-SOFC open circuit potential. However, the net effect of temperature on apparent exchange current densities and Tafel slopes $(RT/(\beta \cdot v_e F))$, where β is the symmetry factor, also need to be taken into account.

Figure 4 shows the calculated effect of temperature on the standard Gibbs energy change $\Delta_r G_T^{\theta}$, standard enthalpy change $\Delta_r H_T^{\theta}$, $T \cdot \Delta_r S_T^{\theta}$ and standard equilibrium potential difference $(\Delta E_T^{\theta} = -\Delta_r G_T^{\theta}/(V_e F))$ for the oxygen driven oxidation of hydrogen to steam:

$$O_2 + 2H_2 \rightleftarrows 2H_2O \quad (1)$$

Coefficients [28] for the polynomial equation describing the empirical temperature dependence of heat capacities at constant pressure enabled calculation of the temperature dependence of the enthalpy and entropy changes for reaction (1) from which the temperature dependence of the equilibrium potential was calculated from Eq. 2 in the usual way:

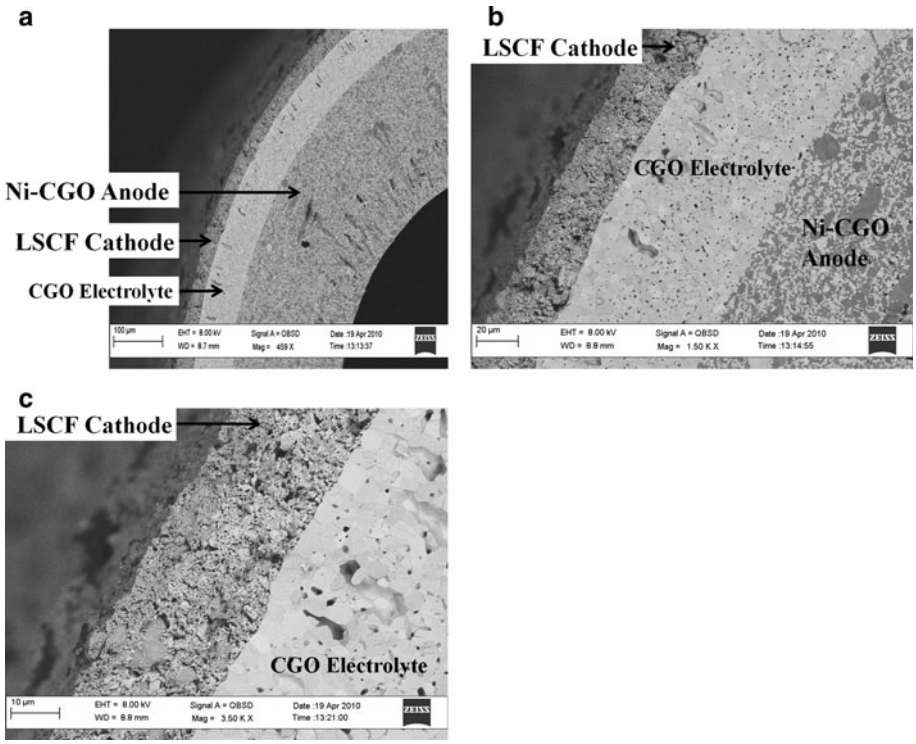

Fig. 2 Photomicrographs taken after reduction of, and experiments with, MT-SOFC, showing cross section: ca. 230 μm porous Ni–CGO inner anode layer, ca. 80 μm dense CGO electrolyte and ca. 30 μm outer porous LSCF cathode

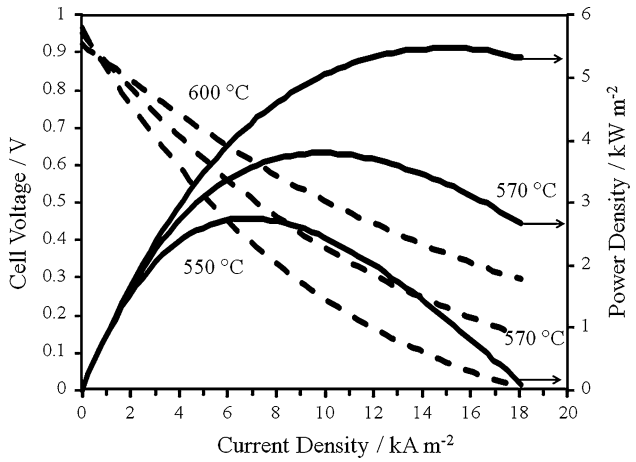

Fig. 3 Effect of temperature on H_2|Ni–CGO|CGO|LSCF|air MT-SOFC performance. Length 25 mm; H_2 flow rate 15 cm^3 min^{-1}; NiO reduction time 150 min at 550 °C

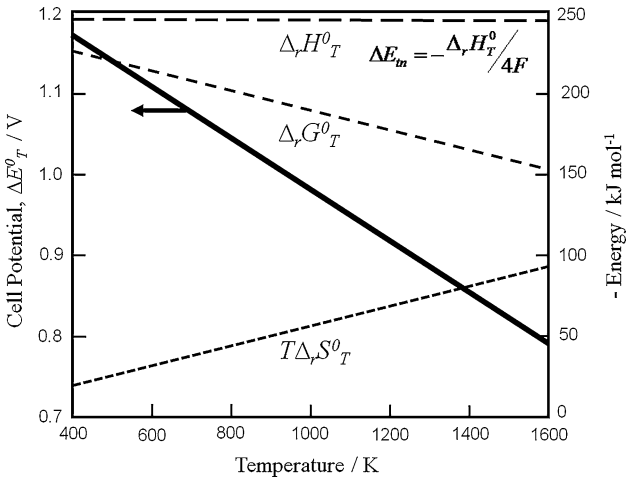

Fig. 4 Effect of temperature on the standard Gibbs energy change ($\Delta_r G_T^\ominus$), standard enthalpy change ($\Delta_r H_T^\ominus$), $T \cdot \Delta_r G_T^\ominus$ and standard equilibrium potential difference ($\Delta E_T^\ominus = -\Delta_r G_T^\ominus/(V_e F)$) for oxygen driven oxidation of hydrogen to steam

$$\Delta E_T = \Delta E_T^\ominus + \frac{RT}{4F}\ln\left\{\frac{P_{H_2}^2 P_{O_2}}{P_{H_2O}^2}\right\} = -\frac{\left(\Delta_r H_T^\ominus - T\Delta_r S_T^\ominus\right)}{4F} + \frac{RT}{4F}\ln\left\{\frac{P_{H_2}^2 P_{O_2}}{P_{H_2O}^2}\right\} \quad (2)$$

Comparison of these predicted equilibrium potential differences with measured open circuit potentials was an important check that (i) the MT-SOFCs did not have cracks or pin-holes in the electrolyte, enabling hydrogen–oxygen recombination or, (ii) at higher temperatures, that electronic conductivity in the CGO did not cause significant short circuiting.

3.3 Effect of hydrogen flow rate on MT-SOFC performance

Figure 5 shows the effect of current density and hydrogen flow rate on the cell voltage and power densities for a

25 mm long H_2|Ni–CGO|CGO|LSCF|air MT-SOFC at 550 °C; the NiO anode precursor had been reduced for ca. 100 min at 550 °C. At current densities >5 kA m^{-2}, increasing the flow rate from 15 to 30 to 60 cm^3 H_2 min^{-1} increased cell voltages and power densities, due to a contribution of anode concentration polarisation to the overall potential losses; a maximum power density of ca. 3 kW m^{-2} was achieved even at 550 °C. As the fuel flow rate was decreased from 60 to 15 cm^3 min^{-1}, mass transfer limited current densities decreased from ca. 13 to ca. 11 kA m^{-2}, leading to precipitously low voltages, caused by local decreases in partial pressure of the reactant at the triple phase boundary sites within the anode, due to diffusion limitations through the anode radial thickness. However, as the anode had been pre-reduced with hydrogen for ca. 100 min at 550 °C, it is probable than NiO was continuing to be reduced during acquisition of the data shown in Fig. 5. Nonetheless, in the order of increasing hydrogen flow rate, each set of data was acquired in 2–3 min (c.f. a pre-reduction time of ca. 100 min), so that the effect of increasing hydrogen flow rate increasing current densities was not influenced significantly by that time. However, comparison of Fig. 5 with data in Figs. 3 and 7, for which anodes were pre-reduced with hydrogen for 150 min at 550 °C, implies that residual NiO was probably still being reduced during the experiments. This was the probable cause of current densities greater than that (ca. 7 kA m^{-2}) corresponding to maximum power in Fig. 5, being lower than those in Figs. 3 and 7 and the appearance in Fig. 5 of an apparent transport controlled current densities as zero cell voltage was approached.

Lower fuel utilisations, corresponding to higher hydrogen flow rates, increased the MT-SOFC performance due to decreased anode activation and concentration polarisations which are inversely related to local hydrogen partial pressures. Morphological changes to the anode microstructure, such as changes to the porosity may increase these limiting current densities and improve MT-SOFC performance; an optimum microstructure exists which leads to the lowest cumulative activation and concentration overpotentials and hence greatest maximum power densities.

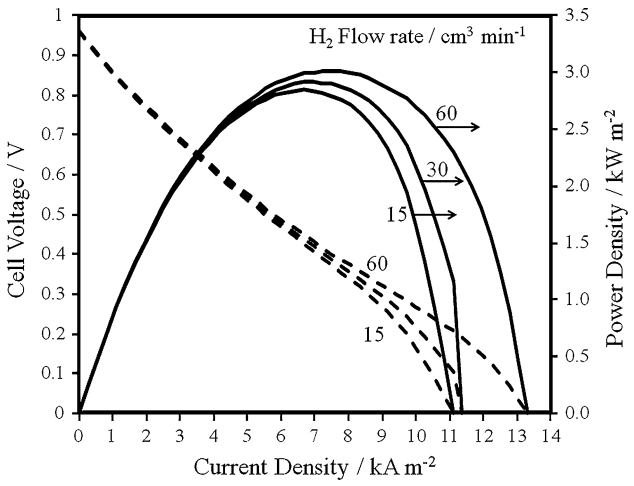

Fig. 5 Effect of hydrogen flow rate on H_2|Ni–CGO|CGO|LSCF|air MT-SOFC performance at 550 °C. Length 25 mm; NiO reduction time ca. 100 min at 550 °C

Low permeability due to the small, distributed sponge-like pores in the anode caused mass transfer of the reactant and product species to be dominated by diffusion. This microstructure was selected to provide increased strength and axial electronic conductivity in the anode, but requires further optimization to achieve higher permeabilities, so mitigating this mass transfer resistance and hence increasing transport limited current densities. The optimum anode microstructure is dictated by the conflicting constraints of maximizing permeability, triple phase boundaries for the reaction and mechanical and thermal robustness of the HF-SOFC. Microstructures that provide high permeability whilst maintaining strength need to be produced to form the bulk of the anode, with a lower porosity, high density of triple phase boundary lengths of order a few micrometres thick close to the electrolyte, forming the active reaction zone. Such microstructures can be produced using the phase inversion process by careful control of the spinning and extrusion parameters of Ni–CGO anode precursors.

3.4 Effect of thermal cycling on MT-SOFC performance

Figure 6 shows the effect of cycling the temperature between a minimum of 300 °C and maximum of 570 °C, on the power density of a 25 mm long H_2|Ni–CGO|CGO|LSCF|air MT-SOFC operating at a cell voltage of 0.5 V and a H_2 flow rate of 15 cm^3 min^{-1}; the original NiO reduction time was 150 min at 550 °C. All temperatures reported were derived from measurements with a K-type thermocouple placed within the quartz reactor close to the HF-SOFC cathode surface. During thermal cycling tests, the HF-SOFC was ramped up to a temperature of 570 °C at 20 °C min^{-1}. However, absence of forced cooling ensured that the cooling rate was ca. 6 °C min^{-1}. Whilst longer term thermal cycling data are desirable to better establish the thermal stability of the HF-SOFCs, 5 cycles were used in this study to indicate initial proof of thermal resilience. Power densities decreased from an initial 4.2–3.8 kW m^{-2} after four cycles, but increased to >4.6 kW m^{-2} when the final steady state temperature was increased to 600 °C after 6 h. The marginal decreases in the performance can be attributed to the furnace not being capable of achieving the set temperature within the set ramp programme, rather than degradation of the MT-SOFC performance, as evidenced

by the performance recovered when the temperature was allowed to equilibrate at 600 °C.

3.5 Effect of NiO reduction time on MT-SOFC performance

Figure 7 shows the effect of time of NiO reduction with H_2 at 550 °C:

$$NiO + H_2 \overset{550\,^{\circ}C}{\longrightarrow} Ni + H_2O \quad (3)$$

on the subsequent effect of current density and hydrogen flow rate on the cell voltage and power densities for a 25 mm long H_2|Ni–CGO|CGO|LSCF|air MT-SOFC at 550 °C with a H_2 flow rate of 15 cm^3 min^{-1}. As the molar volumes at 298 K of NiO and Ni are 11.20 and 6.59 cm^3 mol^{-1}, respectively, the 41% change in molar volume associated with reaction (3) would have produced a significant increase in conductivity and porosity of the MT-SOFC anode, resulting in improved performance with time. Additionally, the cross-sectional microstructure shown in Fig. 2a suggests that the smaller sponge-like pores within the anode dense layer impart superior kinetic performance, but also to some extent impede hydrogen transport into the anode depth, so retarding the reduction of NiO. The complexities of the kinetics of reaction (3) have been reported widely [29–31], NiO conversion being strongly dependent on time and temperature, with an optimum temperature arising from inhibition caused by sintering of the nickel product. Time-resolved XRD of anodes indicated that shorter reduction times led to incomplete conversion of NiO to Ni, leading to decreased active area for the hydrogen oxidation and increased anode electronic resistivity, hence explaining poorer performances with shorted NiO reduction times. Increased reduction times beyond 150 min did not appear to affect the MT-SOFC performance significantly, but their long term stability needs to be established by further study.

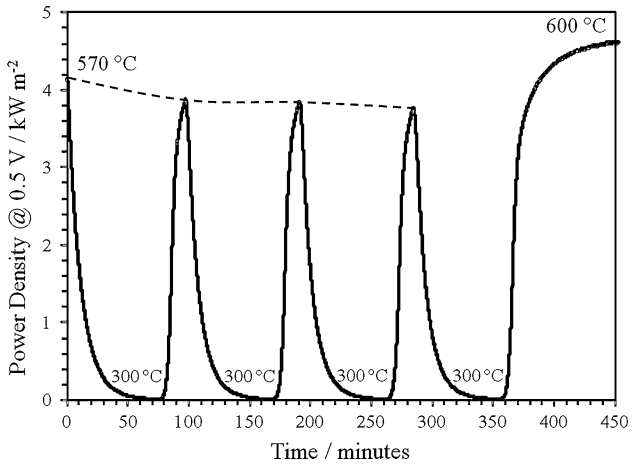

Fig. 6 Effect of thermal cycling on H_2|Ni–CGO|CGO|LSCF|air MT-SOFC performance at cell voltage 0.5 V. Length 25 mm; H_2 flow rate 15 cm^3 min^{-1}; NiO reduction time 150 min at 550 °C. Thermal cycling between a minimum of 300 °C and maximum of 570 °C, with a final steady state temperature of 600 °C

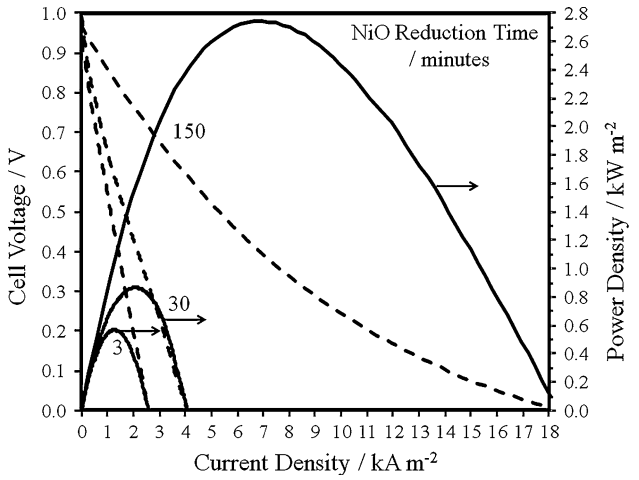

Fig. 7 Effect of time of NiO reduction with H_2 at 550 °C on H_2|Ni–CGO|CGO|LSCF|air MT-SOFC performance at 550 °C. Length 25 mm; H_2 flow rate 15 cm^3 min^{-1}

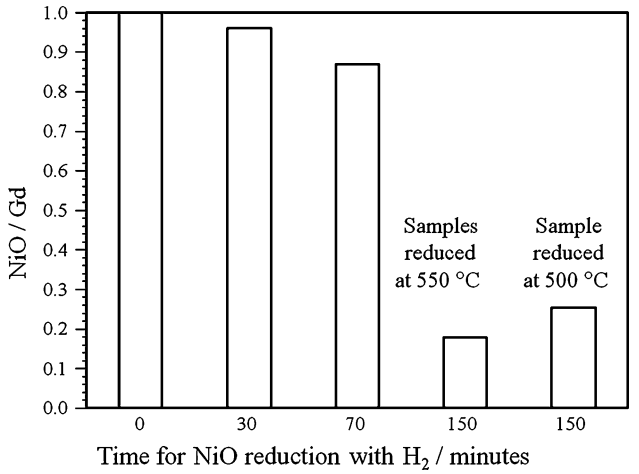

Fig. 8 Effect of time of reduction of NiO with H_2 at 550 °C (and 500 °C), as inferred from NiO/Gd molar ratio determined from diffractograms

Single layer 60 wt% NiO–40 wt% CGO fibres reduced with hydrogen at 550 °C (and 500 °C) and XRD analyses used to determine the residual NiO as a function of time. Figure 8 shows that even after 150 min of reduction, some NiO remained unreduced, which would have affected both anode conductivities and triple-phase boundary lengths. A temperature of 500 °C resulted expectedly in a greater residual amount of NiO after 150 min of reduction in hydrogen, as did NiO with lower porosities and slower hydrogen flow rates.

4 Conclusions

(a) Recent literature has been reviewed on a phase inversion process followed by sintering, used to fabricate ceramic HFs as precursors to MT-SOFCs with sub-millimetre inner diameters.

(b) These exhibited increased electrode surface areas per unit volume relative to their planar or conventional tubular SOFC counterparts, thereby increasing power outputs per unit volume/mass, facilitating sealing at high temperatures, and decreasing fabrication costs per kW.

(c) Micro-tubular SOFCs produced by co-extrusion followed by phase inversion of HFs that were sintered subsequently have shown promising performance at 'intermediate' temperatures of 500–600 °C.

(d) The effects were reported of temperature, hydrogen flow rate, thermal cycling and time of NiO reduction with H_2 on the performance of 25 mm long H_2|Ni–CGO|CGO|LSCF|air MT-SOFCs, incorporating CGO electrolyte, nickel anodes and LSCF cathodes, designed to operate at 500–600 °C. Maximum power densities of 3–5.5 kW m^{-2} were achieved, depending on hydrogen flow rate, after the NiO anode precursor had been reduced with hydrogen at 550 °C for >150 min, thereby increasing effective anode conductivities and increasing porosities.

Acknowledgments The authors thank the UK Engineering and Physical Sciences Research Council and the British Council for studentships for ND and UD, respectively.

References

1. Grande FD, Thursfield A, Kanawka K, Droushiotis N, Doraswami U, Li K, Kelsall GH, Metcalfe IS (2009) Solid State Ion 180(11–13):800
2. Droushiotis N, Doraswami U, Kanawka K, Kelsall GH, Li K (2009) Solid State Ion 180(17–19):1091
3. Howe KS, Thompson GJ, Kendall K (2011) J Power Sources 196:1677
4. Droushiotis N, Doraswami U, Kelsall GH (2009) Trans Electrochem Soc 25(2):1241
5. Brett DJL, Atkinson A, Brandon NP, Skinner SJ (2008) Chem Soc Rev 37:1568
6. Othman MdHD, Droushiotis N, Wu Z, Kelsall GH, Li K (2011) J Power Sources 196:5035
7. Othman MdHD (2011) High performance micro-tubular solid oxide fuel cell, PhD Thesis, Imperial College London
8. Doraswami U, Droushiotis N, Kelsall GH (2010) Electrochim Acta 55:3766
9. Doraswami U (2010) Modelling of micro-tubular hollow fibre solid oxide fuel cells. PhD Thesis, Imperial College London
10. Droushiotis N, Othman MdHD, Doraswami U, Wu Z, Kelsall GH, Li K (2009) Electrochem Commun 11:1799
11. Droushiotis N, Doraswami U, Kelsall GH (2009) Trans Electrochem Soc 25(2):665
12. Othman MdHD, Wu Z, Droushiotis N, Doraswami U, Kelsall GH, Li K (2010) J Membr Sci 351:196
13. Droushiotis N, Doraswami U, Ivey D, Othman MdHD, Li K, Kelsall GH (2010) Electrochem Commun 12:792
14. Othman MdHD, Droushiotis N, Wu Z, Kelsall GH, Li K (2011) Advanced materials 23:2480
15. Droushiotis ND (2011) Fabrication and characterization of hollow fibre micro-tubular solid oxide fuel cells. PhD Thesis, Imperial College London
16. Othman MdHD, Droushiotis N, Wu Z, Kanawka K, Kelsall GH, Li K (2010) J Membr Sci 365(1–2):382
17. Othman MdHD, Wu Z, Droushiotis N, Kelsall GH, Li K (2010) J Membr Sci 360(1–2):410
18. Doraswami U, Shearing P, Droushiotis N, Li K, Brandon NP, Kelsall GH (2009) Solid State Ion 192:494
19. Yang NT, Tan XY, Ma ZF (2008) J Power Sources 183:14
20. Yang C, Li W, Zhang S, Bi L, Peng R, Chen C, Liu W (2009) J Power Sources 187:90
21. Jin C, Liu J, Li LH, Bai YH (2009) J Membr Sci 341:233
22. Zhang X, Lin B, Ling Y, Dong Y, Meng G, Liu X (2010) Int J Hydrog Energy 35:8654
23. Yang C, Jin C, Chen F (2010) Electrochim Acta 56:80
24. Zhao L, Zhang X, Hea B, Liu B, Xia C (2011) J Power Sources 196:962
25. Kendall K (2009) Int J Appl Ceram Technol 7:1
26. Suzuki T, Yamaguchi T, Fujishiro Y, Awano M (2006) J Power Sources 160:73
27. Suzuki T, Funahashi Y, Yamaguchi T, Fujishiro Y, Awano M (2008) J Alloys Compd 451:632
28. NIST-JANAF (1998) Thermochemical tables, 4th edn. J Phys Chem Ref Data Monogr 9:1–1951. http://webbook.nist.gov/chemistry/. Accessed 24 July 2011
29. Song HY, Wadsworth ME (eds) (1979) Rate processes in extractive metallurgy. Plenum, New York, pp 303
30. Szekely J, Evans JW (1971) Chem Eng Sci 26:1901
31. Szekely J, Evans JW (1973) Chem Eng Sci 28:1975